Modes of sea-water intrusion during transgression.

Kooi, H.; Groen, J.

published in
Water Resources Research
2000

DOI (link to publisher)
10.1029/2000WR900243

document version
Publisher's PDF, also known as Version of record

WATER RESOURCES RESEARCH, VOL. 36, NO. 12, PAGES 3581–3589, DECEMBER 2000

Modes of seawater intrusion during transgressions

H. Kooi and J. Groen

Faculty of Earth Sciences, Vrije Universiteit, Amsterdam

A. Leijnse[1]

National Institute of Public Health and Environmental Protection, Bilthoven, Netherlands

Abstract. Analytical methods and numerical experiments are used to study salinization of groundwater in response to sea level rise. The system that is studied involves a saturated porous medium with an inclined upper surface. The upper surface is progressively inundated during sea level rise to simulate transgression, the landward migration of the shoreline. Four "modes" of seawater intrusion are distinguished: (1) horizontal intrusion for slow transgression and a relatively high-permeability (sand/silt) substrate, (2) vertical intrusion by seawater fingering for fast transgression and a sand/silt substrate, (3) vertical intrusion by diffusion for fast transgression and a low-permeability (clay) substrate, (4) vertical intrusion by combined diffusion and low-salinity fingering for fast transgression and a clay layer at the seafloor overlying an aquifer. These four modes are characterized by the development of very distinctive transition zones between the fresh and salt groundwater domains. An analytical expression is derived for the critical transgression rate which separates horizontal (mode 1) from dominantly vertical (modes 2–4) intrusion. For modes 3 and 4, salinization significantly lags behind sea level rise. The results are consistent with observations of fossil fresh/brackish groundwater beneath many continental shelves and shallow seas.

1. Introduction

The present distribution of fresh and salt groundwater in coastal aquifer systems has been shaped by natural processes operating at geological timescales and, more recently, by human activities in the coastal zone. Of these two factors, the influence of man's interference on salinity patterns has received by far the greatest attention in hydrological studies [e.g., *Souza and Voss*, 1987; *Galeati et al.*, 1992; *Bear et al.*, 1999]. These studies have led to a rather thorough understanding of phenomena such as seawater intrusion and upconing of fresh-salt interfaces induced by groundwater extraction and other engineering activities. In comparison, process-based knowledge of the natural, geological changes that were responsible for shaping preinterference conditions is still relatively limited.

Some of the changes in salinity patterns brought about by geological processes can be readily recognized in the current salinity distribution. Examples are entrapped old seawater in and below clay-rich formations in present onshore areas [*Manheim and Horn*, 1968; *De Vries*, 1981; *Custodio et al.*, 1987] and fossil fresh/brackish groundwater far offshore [e.g., *Kohout et al.*, 1977; *Hathaway et al.*, 1979; *Manheim and Paull*, 1981; *Groen et al.*, 2000]. Figure 1 shows two of the latter relatively fresh groundwater occurrences at the continental margins of Suriname and of the United States at New Jersey. These salinity patterns are not in equilibrium with present-day boundary conditions, but transient features which form relics of former, different boundary conditions, notably sea levels that were higher and lower than today. Apparently, the response of the subsurface water quality distribution to sea level change often is sufficiently slow to allow the development of these relics.

The question arises as to whether this conceptual picture of disequilibrium adjustment to sea level change can be understood quantitatively. In the present paper this question is addressed for the specific case of sea level rise, which characterizes the most recent geological time period, the Holocene (last 10,000 years), during which sea level rose by >100 m and landward shifts of coastlines over tens to hundreds of kilometers occurred on most continental shelves and other shallow seas. Both analytical methods and numerical experiments are used to study the style of seawater intrusion during sea level rise and the factors that favor a large lag in response. In the analysis, transgression, the landward migration of the coastline in response to sea level rise, which is of paramount importance at geological timescales, is explicitly taken into account.

Only a few studies have previously addressed seawater intrusion due to sea level rise quantitatively, and they differ strongly in adopted approach. In all these studies, modeling has remained rather tractable because potentially unstable density stratification of seawater overlying fresh groundwater was either avoided or ignored because of the assumptions made. *Kana et al.* [1984] used the steady state, sharp interface, Badon Ghijben-Herzberg approximation in a study of the coastal area of South Carolina and represented temporal evolution by a series of steady state configurations for different sea levels. *Meisler et al.* [1984] used a similar approach to study the effects of sea level change at geological timescales on the continental shelf off New Jersey but relaxed the Badon Ghijben-Herzberg assumption of hydrostatic pressure conditions in the freshwater domain. *Navoy* [1991] calculated transient saltwater intrusion due to increased salinity of the Delaware

[1]Now at National Institute of Applied Geosciences, Utrecht, Netherlands.

Paper number 2000WR900243.
0043-1397/00/2000WR900243$09.00

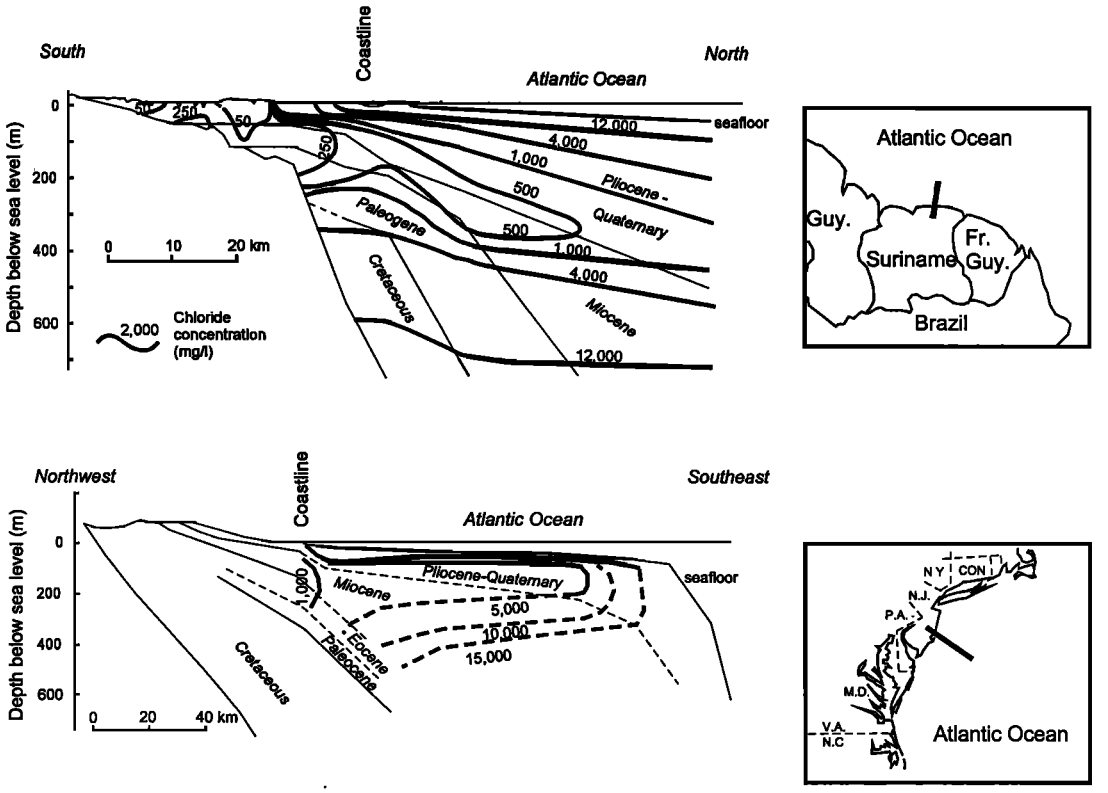

Figure 1. Examples of relatively fresh groundwater extending far into the offshore. (top) Continental margin of Suriname, South America [modified after *Groen et al.* 2000]. (bottom) U.S. Atlantic continental margin off New Jersey [modified after *Hathaway et al.*, 1979]. Thick lines denote contours of chloride concentrations (mg/L). Seawater chlorinity is typically ~19,000 mg/L.

River. Transport calculations included the development of a diffuse transition zone, but fluid density was assumed to be uniform. *Oude Essink* [1996, 1999] used fully transient, variable-density flow and transport calculations of seawater intrusion in the coastal area of Netherlands in response to various scenarios of future sea level rise but did not consider a horizontal shift of the coastline. This neglect of coastline migration in his studies is reasonable given the occurrence of coastal defence measures maintaining the coastline at a relatively fixed position and given the small magnitude of sea level rise considered. The present work is concerned with fully transient, variable-density flow and transport and focuses specifically on the role of transgression.

First, some simple analytical results are presented, which suggest the existence of a critical rate of transgression which separates a domain of predominantly horizontal seawater intrusion (horizontal migration transition zone) from predominantly vertical seawater intrusion by fingering and diffusion. These two styles occur for transgression rates that are lower (in the following referred to as subcritical) and higher (referred to as supracritical) than the critical transgression rate, respectively. Then, a series of numerical model experiments are presented which illustrate the various modes of seawater intrusion for different controls in greater detail. Subsequently, the results are generalized into a scheme in which a limited number of modes of seawater intrusion are distinguished together with their controls. Finally, using this scheme, the factors favoring preservation of fresh/brackish groundwater in the offshore are inferred and discussed in relation to observational data.

2. Critical Transgression Rate Controlling Vertical Seawater Intrusion

It has been known for many decades that the steady state distribution of groundwater salinity in a coastal aquifer typically takes the form of a landward dipping seawater wedge that is separated from the freshwater domain by a transition zone of finite width resulting from diffusion and dispersion [e.g., *Henry*, 1964]. The top of the wedge coincides with the coastline, and both the geometry of the wedge (for instance, dip angle) and the width of the transition zone are a function of dispersivity, freshwater hydraulic gradient (freshwater recharge to the coast), and permeability distribution [*Volker and Rushton*, 1982; *Reilly and Goodman*, 1985]. Obviously, if the coastline moves some distance inland owing to sea level rise (transgression), ultimately, the wedge will assume a new steady state, in equilibrium with the new location of the coastline. It can be readily envisaged that if the transgression is sufficiently slow, a quasi-steady evolution results in which the temporal evolution of the salinity distribution can be approximated by a series of steady state wedges, in equilibrium with the momentary location of the coastline. Consequently, under these circumstances seawater intrusion into the former coastal zone is effectively horizontal. The rate at which the subsurface saltwater wedge can migrate horizontally by advection is, inherently, limited by the aquifer permeability. Therefore it follows that if the rate of transgression is sufficiently fast, the seawater wedge in the subsurface will not be able to keep up and seawater will move on top of the fresh groundwater domain, causing seawater

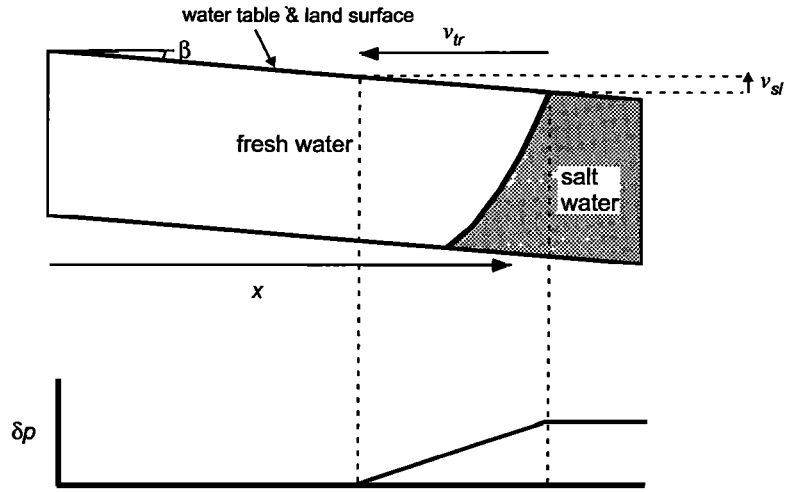

Figure 2. Schematic illustration of geometry and variables used in the analysis of section 2.

intrusion top down by diffusion and, possibly, fingering. Fingering here refers to narrow "plumes" of salt water descending into the subsurface resulting from the unstable nature of the density stratification when salt water occurs on top of fresh water [e.g., *Wooding et al.*, 1997]. These convective flow features cause a much more rapid salinization than diffusion and can carry salts to great depths over short timescales. The above implies that the transition from predominantly horizontal to vertical seawater intrusion is controlled by a critical rate of transgression. This concept will be investigated in detail by numerical experiments in section 3. In this section a simple analytical estimation of the critical transgression rate is derived.

Figure 2 schematically shows the geometry that is being considered. An aquifer and land surface dip seaward at angle β. The initial coastline and the associated steady state saltwater wedge are indicated also. It is assumed that the onshore water table coincides with the land surface. That is, processes in the unsaturated zone are neglected. This seems reasonable because the low transgression rates considered in this study are unlikely to carry seawater on top of the vadose zone as tidal and wave movements do. If the rate of sea level rise is denoted by v_{sl}, the rate of transgression is given by

$$v_{tr} = v_{sl}/\tan \beta. \tag{1}$$

Let the steady state flow field $\mathbf{q}^*$ be given by

$$\mathbf{q}^* = -\frac{\mathbf{k}}{\mu}(\nabla p^* + \rho^* \mathbf{g}), \tag{2}$$

where the asterisk refers to steady state, $\mathbf{k}$ is the intrinsic permeability tensor, μ is fluid viscosity, p is pore pressure, ρ is fluid density, $\mathbf{g}$ is gravitational acceleration, and ∇ is the gradient operator. An instantaneous small amount of sea level rise will induce a perturbation of the pore pressure field δp, such that the new flow field can be written as

$$\mathbf{q} = -\frac{\mathbf{k}}{\mu}[\nabla(p^* + \delta p) + \rho^* \mathbf{g}] = \mathbf{q}^* - \frac{\mathbf{k}}{\mu}\nabla \delta p, \tag{3}$$

where the second term on the right-hand side denotes the perturbation of the flow field that is responsible for advection of the salinity distribution. At the top boundary of the aquifer, δp is simply given by the change in weight of the seawater column. This is shown schematically in Figure 2. The horizontal gradient of δp at the surface is given by $d\delta p/dx|_{\text{surf}} \approx \rho_{\text{sea}} g \tan \beta$, (we are interested in absolute, scalar values, so we drop signs and vector/tensor notation here and in the following). It does not depend on the magnitude of sea level rise but on the gradient of the land surface only. In general, the magnitude of $d\delta p/dx$ will decrease with depth in the aquifer. Therefore an upper bound to the horizontal rate of advection of the fresh-salt interface due to the pressure perturbation associated with sea level rise is given by

$$v_{\text{adv}}^{\max} = \frac{k}{n\mu} \rho_{\text{sea}} g \tan \beta, \tag{4}$$

where n is aquifer porosity. Equation (4) provides an estimate for the critical transgression rate $v_{tr}^{cr} = v_{\text{adv}}^{\max}$. If $v_{tr} \gg v_{tr}^{cr}$, the saltwater wedge in the aquifer is expected not be able to keep up with the migrating shoreline. This behavior may also be expressed in nondimensional terms by combining (1) and (4)

$$\Gamma = v_{tr}/v_{tr}^{cr} = \frac{n\mu v_{sl}}{k\rho_{\text{sea}} g \tan^2 \beta}, \tag{5}$$

where the critical value is expected at $\Gamma^{cr} \approx 1$. Equation (5) shows that high values of Γ, which would favor the lagging behind of the saltwater wedge, tend to occur for large values of v_{sl}, low permeability k, and, in particular, low-gradient land surfaces tan β.

In the above derivation, only the pressure perturbation associated with sea level rise was considered. Adjustments in the salinity distribution will also contribute to the flow field. These effects are addressed in the numerical investigation reported in section 3. Equations (4) and (5) serve as a frame of reference or working hypothesis for the numerical experiments.

3. Numerical Investigation

3.1. Numerical Code

The numerical experiments reported in this paper were conducted with the finite element, variable-density flow and transport code METROPOL-3. For a detailed description of the code the reader is referred to the works by *Leijnse* [1992], *Sauter et al.* [1993], *Leijnse and Oostrom* [1994], or *Oostrom et al.* [1994]. The code solves two coupled partial differential

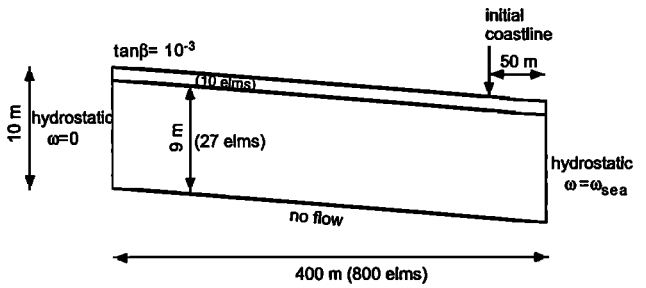

Figure 3. Geometry, mesh, and boundary conditions used in the numerical model experiments (not to scale).

equations in salt mass fraction, ω and fluid pressure p. The equations are nonlinear because the fluid properties ρ and μ depend on ω. The equations are coupled through $\mathbf{q}$ and ρ. Here we use a constant value for μ because of the low salt mass fractions considered. For fluid density, $\rho = \rho_0 e^{\gamma\omega}$ is used, where ρ_0 is the freshwater density and $\gamma = 0.69$. The latter value gives fluid densities deviating <0.1% from experimental values for salt mass fractions varying from $\omega = 0$ (fresh water) to $\omega = 0.26$ (saturated brine) [*Leijnse*, 1992]. Fluid and pore compressibilities are neglected, corresponding to zero specific storage. This is reasonable given that the changes in pressure boundary conditions occur only very slowly.

The numerical scheme uses the Galerkin weighted residual finite element method, fully implicit backward time stepping with automatic time step control based on convergence requirements. A consistent velocity formulation is used to represent Darcy velocities [*Voss and Souza*, 1987]. METROPOL-3 has been compared with other codes for a number of benchmark problems in the HYDROCOIN project [*Leijnse and Hassanizadeh*, 1989a, 1989b] and was found to give comparable results.

3.2. Experimental Setup

Model experiments are carried out on a two-dimensional vertical cross section with a geometry similar to that of Figure 2. Geometry and boundary conditions are shown in Figure 3. Because of numerical limitations (detailed below), the dimensions of the section (400 m wide, 10 m high) are small compared to the width of continental shelves (typically 100 km) and brackish water occurrences several hundreds of meters below the seafloor. Also, the simulated timescales (200–2000 years) do not cover the entire Holocene period. However, the basic styles of seawater intrusion that can develop are well illustrated even at these reduced scales. Moreover, from the experiments and the discussion presented in section 2 it can be readily understood how salinization at larger space and timescales will occur.

The gradient of the topographic surface in the experiments is tan $\beta = 10^{-3}$, which is a typical mean value for continental shelves (100 m water depth at a shelf edge for a 100 km wide shelf). The finite-element mesh consists of 29,600 quadrilateral elements; 800 in the horizontal and 37 in the vertical direction. The horizontal element size is uniform with $\Delta x = 0.5$ m. The vertical element size in the top 1 m of the section is $\Delta z = 0.1$ m; below this layer, $\Delta z = 1/3$ m. The maximum time step employed is 10^7 s, which keeps Courant number smaller than 1 at all times. The bottom of the domain is a no-flow and no-diffusion boundary. At the left boundary, freshwater conditions and a hydrostatic pressure distribution are imposed. The conditions at the top and right boundary are time dependent, depending on sea level. The right boundary is assigned hydrostatic pressure conditions and a constant seawater salinity. The pressure part of the top boundary condition is given by

$$p_b = \rho_{sea} g h(t) | h(t) \geq 0 \qquad p_b = 0 | h(t) < 0, \tag{6}$$

where p_b is the boundary fluid pressure and $h(t)$ is the local sea depth. The influence of tidal fluctuations is not taken into account. The section is assumed fully saturated such that the topographic gradient controls the onshore hydraulic pressure gradient.

A time-dependent Dirichlet boundary condition is used for ω at the top boundary:

$$\omega_b = \omega_{sea} | h(t) \geq 0 \qquad \omega_b = 0 | h(t) < 0. \tag{7}$$

Strictly speaking, this method is not very physical as, over time, salt is introduced in the top elements of the finite element mesh (because ω varies linearly within an element), which is not accounted for by boundary fluxes. However, as long as the vertical mesh size Δz is small, the "mass balance error" is also small (moreover, its cause is known). More importantly, in order to achieve convergence in the calculations, $\Delta z < \delta_{cr}$, where δ_{cr} denotes the thickness of the saline boundary layer at the top of the domain at the instant it becomes unstable and fingers start to develop, which occurs when the boundary layer reaches a finite thickness. This implies that the Rayleigh number for a boundary layer with length (thickness) scale Δz has to be smaller than the critical boundary layer Rayleigh number, or

$$\frac{\Delta\rho g k \Delta z}{\mu D} < \left(Ra_{cr} = \frac{\Delta\rho g k \delta_{cr}}{\mu D} \right), \tag{8}$$

where $\Delta\rho = \rho_{sea} - \rho_0$, g and k are absolute values of gravitational acceleration and (isotropic) permeability, and D is the scalar value of an assumed isotropic dispersion tensor. Effects of porosity n and tortuosity τ are accounted for in the way D is defined in the model $D = nD^*/\tau^2$, with D^* being the diffusivity in water (mechanical dispersion ignored). If $\Delta z > \delta_{cr}$, the boundary layer that is created numerically just below the seafloor is always unstable (its Rayleigh number is larger than critical). Hence, under these circumstances, fingering starts too early in the model. More crucial, however, upward seepage of fresh water into the sea tends to create a boundary layer of finite thickness $\delta = D/q$, which is more compressed if the upflow is stronger [*Wooding et al.*, 1997]. If the upflow is strong enough, the boundary layer is compressed to such an extent that it remains stable at all times. Hence, under these conditions, insufficient spatial discretization $\Delta z > \delta_{cr}$ will create an unstable boundary layer and fingering in the model unjustly. *Wooding et al.* [1997] found $Ra_{cr} \approx 10$ from both perturbation analyses and numerical and Hele-Shaw cell experiments.

Similarly, Δx has to be chosen such that the critical wavelength of boundary layer instabilities λ_{cr}, which controls the dimensions of finger instabilities, is resolved. Because $\lambda_{cr} \approx 15\delta_{cr}$ [*Wooding et al.*, 1997], the following is appropriate:

$$\Delta x < (\tfrac{1}{8}\lambda_{cr} \approx 2\delta_{cr} = 2Ra_{cr}\mu D/\Delta\rho g k). \tag{9}$$

The validity of the above conditions was corroborated for the "long-heater" Elder problem [*Elder*, 1968] (seawater conditions along the entire width of the top of the domain) with and without upflow. That is, numerical experiments were performed to test (1) grid/mesh convergence and (2) $Ra_{cr} \approx 10$. Without upflow, progressive refinement of the mesh, both in

Table 1. Summary of Numerical Experiments

Experiment	Lithology	v_{sl}, mm/yr	Γ_{sand}	Γ_{clay}	k_{clay}, m^2	α_L, m	α_T, m	Intrusion
1	sand	0.1	0.93	...	...	10^{-3}	10^{-3}	horizontal
2	sand	0.2	1.86	...	...	10^{-3}	10^{-3}	horizontal
3	sand	0.5	4.65	...	...	10^{-3}	10^{-3}	horizontal
4	sand	0.6	5.58	...	...	10^{-3}	10^{-3}	horizontal
5	sand	0.7	6.51	...	...	10^{-3}	10^{-3}	vertical
6	sand	0.8	7.44	...	...	10^{-3}	10^{-3}	vertical
7	sand	1.0	9.30	...	...	10^{-3}	10^{-3}	vertical
8	sand	1.0	9.30	...	...	10^{-1}	10^{-2}	vertical
9	sand	1.0	9.30	...	...	10^{0}	10^{-1}	vertical
10	sand	0.6	5.58	...	...	10^{0}	10^{-1}	horizontal
11	sand	0.7	6.51	...	...	10^{0}	10^{-1}	horizontal
12	sand	0.8	7.44	...	...	10^{0}	10^{-1}	vertical
13	clay	1.0	...	9.3×10^{4}	10^{-17}	10^{-3}	10^{-3}	vertical
14	clay	1.0	...	9.3×10^{3}	10^{-16}	10^{-3}	10^{-3}	vertical
15	sand/clay	0.1	0.93	9.3×10^{3}	10^{-17}	10^{-3}	10^{-3}	horizontal
16	sand/clay	0.2	1.86	1.9×10^{4}	10^{-17}	10^{-3}	10^{-3}	vertical
17	sand/clay	1.0	9.30	9.3×10^{4}	10^{-17}	10^{-3}	10^{-3}	vertical
18	sand/clay	1.0	9.30	9.3×10^{3}	10^{-16}	10^{-3}	10^{-3}	vertical
19	sand/clay	1.0	9.30	9.3×10^{4}	10^{-17}	10^{-1}	10^{-2}	vertical
20	sand/clay	1.0	9.30	9.3×10^{4}	10^{-17}	10^{0}	10^{-1}	vertical

the horizontal and vertical direction, and reduction of time stepping indeed resulted in converged solutions where the location of individual fingers varied, but their characteristic wavelength and growth rate became constant. Too coarse discretization led to a different timing of instability development and finger dimensions that were too large. Insufficient horizontal discretization was found to have a stabilizing effect, causing finger development to be delayed and finger widths equal to the element size. Convergence was also achieved when upflow was imposed for the above problem. Stable boundary layers occurred for boundary layer Rayleigh numbers of 7 and smaller, consistent with the results of *Wooding et al.* [1997]. Too coarse vertical discretization here led to fingering and salinization unjustly. The grid convergence shows that the dynamics of the numerical system is governed by physics and not by the particular realization of "noise" (in our case, truncation errors in the code) which seeds boundary layer instability. This contrasts with recent findings of *Simmons et al.* [1999], who suggest that in applying the SUTRA code to *Wooding et al.*'s [1997] salt lake problem it is inappropriate to rely on round off errors. The cause for this difference is unclear. Recently, *Kolditz et al.* [1998] showed grid convergence for the "short-heater" Elder problem, apparently also relying on round off errors. The grid size for which they obtain a converged solution agrees with (8) and (9).

For the following set of experiments the mesh size was chosen to satisfy (8) and (9) with dispersion dominated by molecular diffusion (substitution of the parameters listed in Table 1 in (8) and (9) and using $Ra_{cr} = 7$ yields $\Delta z < 0.28$ m and $\Delta x < 0.56$ m, respectively). This should ensure proper discretization for simulations in which D includes hydrodynamic dispersion as well. Each experiment starts with the steady state salinity distribution and flow field for a sea level of +0.05 m, which corresponds to a coastline location 50 m from the right boundary of the mesh. Model experiments simulate subsequent salinization for a given rate of sea level rise.

3.3. Results

The experiments that were conducted are summarized in Table 1. In the experiments the following parameters or conditions were varied: (1) a full sand layer, a full clay layer, and a clay layer overlying a sandy aquifer were considered; (2) rate of sea level rise v_{sl}; (3) clay permeability k_{clay}; and (4) longitudinal and transversal dispersivity α_L and α_T. Parameter values that were kept constant are given in Table 2. The term "sand" is used here and in the following to denote sediments with permeabilities that are high relative to clays. The value listed in Table 2 would correspond to the permeability of a fine sand or silt. Using a higher permeability would imply a major increase in numerical cost, as explained in section 3.2. Γ_{sand} and Γ_{clay} denote the nondimensional transgression rate of (5) substituting sand and clay permeability, respectively.

Experiments 1–7 constrain the critical transgression rate Γ^{cr} for a uniform sand substrate and very small hydrodynamic dispersion (>40 times smaller than molecular diffusion). Γ^{cr} for this set of experiments was found to occur between 5.58 and 6.51 (Table 1). Figure 4 displays the horizontal style of salinization for experiment (1). It shows that the transition zone quickly assumes a steeper and narrower geometry during its lateral migration in comparison with the initial steady state situation. It was found that this effect is stronger for higher rates of sea level rise. The observed steepening is probably due to inhibited outflow at the landward side of the transition zone and therefore enhanced input of salt at the top of the transition zone. This steepening, in turn, enhances the clockwise vortex in the flow field associated with the density distribution, which tends to flatten the transition zone. Apparently, the two effects (input of salt at the seafloor and the enhanced clockwise vortex) work together to (1) maintain a constant shape of the transition zone and (2) provide a mechanism for lateral migra-

Table 2. Constant Parameter Values

Parameter	Value	Units
n	0.3	
ω_{sea}	0.0357	
ρ_o	10^3	kg/m^3
k (sand)	10^{-13}	m^2
μ	10^{-3}	Pa s
g	10	m/s^2
D_m	10^{-9}	m^2/s

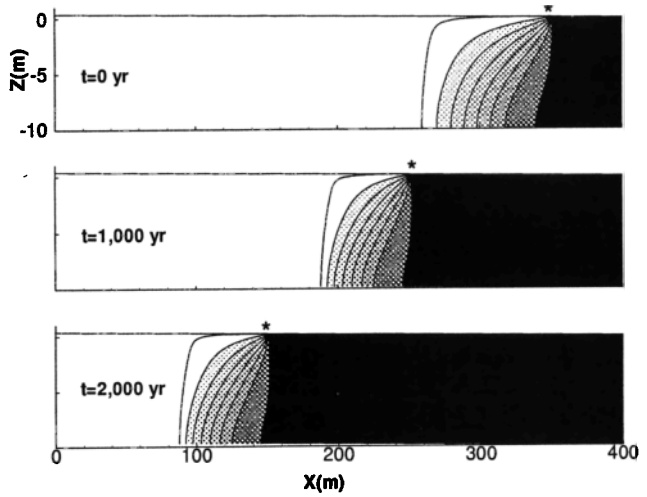

Figure 4. Experiment 1. Calculated salinity distribution at three time steps for a sandy substrate in combination with a subcritical transgression rate. Salt mass fraction increases with darkness of shading. Contours shown are from $\omega = 0.0005$ to 0.0355 at uniform intervals. The current location of the shoreline is indicated by an asterisk. Details are given in the text.

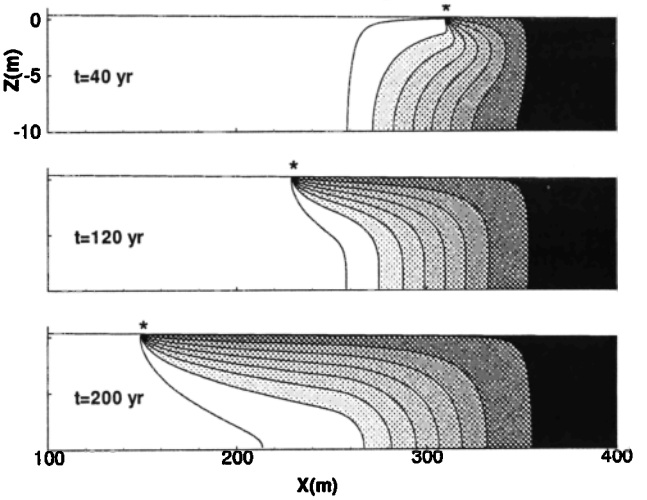

Figure 6. Experiment 13. Calculated salinity distribution at three time steps for a clay substrate in combination with a supracritical transgression rate. Salt mass fraction increases with darkness of shading. Contours shown are from $\omega = 0.0005$ to 0.0355 at uniform intervals. The current location of the shoreline is indicated by an asterisk. Left 100 m of model domain are not shown. Details are given in the text.

tion of the transition zone in addition to that due to the changing pressure boundary conditions at the land surface. The latter effect probably explains why the experimentally determined value of Γ^{cr} of ~6 is larger than the value of 1 predicted in section 2.

Figure 5 shows the salinization history for experiment 7. In this experiment the transition zone lags behind the migrating coastline, and seawater fingers emanate from a diffusive boundary layer which develops as a "moving wave" at the top of the aquifer as seawater overrides fresh groundwater (this boundary layer is seen more clearly in Figure 6, where it remains stable because of low permeability). Theoretically, fingering only starts where this boundary layer reaches a critical thickness. In Figure 7 this occurs close to the current shoreline because the critical thickness is very small; using (8) and adopting $Ra_{cr} = 7$ yields $\delta_{cr} = 0.28$ m. Seawater fingers sink to the base of the aquifer and, in between, freshwater escapes upward into the sea. As a result, a wide, high-salinity transition zone develops between the former and new coastline. Very little flow occurs in this zone once the fingers reach the base of the aquifer, and consequently, the subsequent development of this zone toward full seawater quality is dominated by diffusion and therefore is very slow. In Figure 5 the frontal fingers are de-

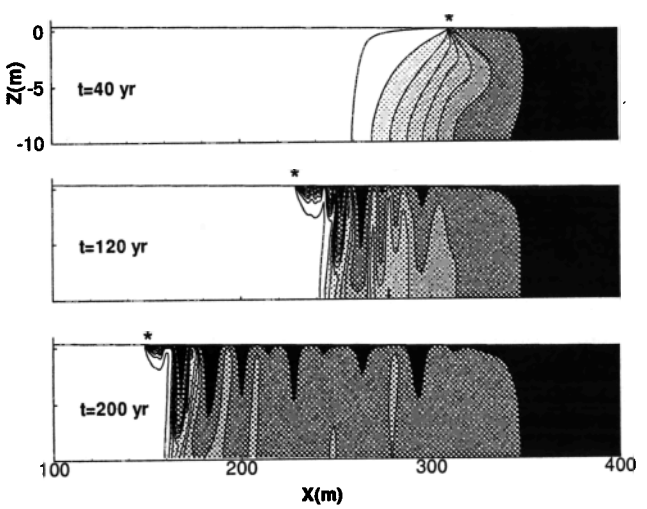

Figure 5. Experiment 7. Calculated salinity distribution at three time steps for a sandy substrate in combination with a supracritical transgression rate. Salt mass fraction increases with darkness of shading. Contours shown are from $\omega = 0.0005$ to 0.0355 at uniform intervals. The current location of the shoreline is indicated by an asterisk. Left 100 m of model domain are not shown. Details are given in the text.

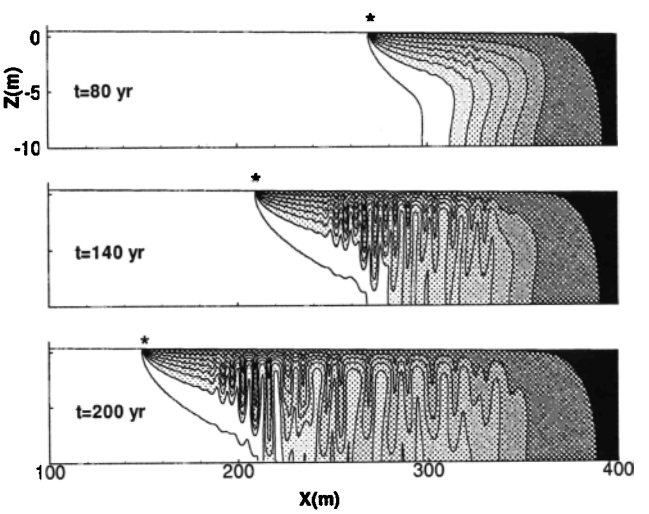

Figure 7. Experiment 17. Calculated salinity distribution at three time steps for a sandy aquifer overlain by a 0.5 m thick clay layer in combination with a supracritical transgression rate. Salt mass fraction increases with darkness of shading. Contours shown are from $\omega = 0.0005$ to 0.0355 at uniform intervals. The current location of the shoreline is indicated by an asterisk. Left 100 m of model domain are not shown. Details are given in the text.

flected somewhat landward as they descend deeper into the aquifer.

In experiments 8–12 the role of hydrodynamic dispersion is investigated. Experiments 8 and 9 are the same as experiment 7, except for increased dispersivities. In experiment 9, with largest dispersivities, $\alpha_L = 1$ m and $\alpha_T = 0.1$ m, respectively, fingers emanate from a thicker saline boundary layer, and finger dimensions are ~3 times larger than in experiment 7, but the basic style of seawater intrusion is not altered. Experiments 10–12, which correspond with experiments 4–6, show that hydrodynamic dispersion slightly increases Γ^{cr} to a value between 6.51 and 7.44.

Experiments 13 and 14 investigate salinization of a uniform clay substrate. In these experiments, vertical "intrusion" by diffusion dominates. Figure 6 illustrates the "moving wave behavior" of the diffusive boundary layer that develops below the seafloor for experiment 13. Owing to the low permeability of the clay the boundary layer stays intact. Not surprisingly, a seaward dipping freshwater wedge develops in the offshore.

The set of experiments 15–20 were conducted for a substrate in which a 0.5 m thick clay layer overlies a sandy aquifer. Figure 7 illustrates the salinization history for experiment 17, which apart from the 0.5 m thick clay layer, is the same as the experiment of Figure 5. The clay layer affects the results in several ways. First, because of its low permeability, the high-salinity part of the diffusive boundary layer which develops within the clay layer is stable (see also Figure 6). Instabilities germinate beneath the clay layer, where the diffusive boundary layer within the aquifer has reached a critical thickness. Second, this critical thickness is larger than for a uniform sandy substrate ($\delta_{cr} > 0.28$ m) because (1) the density contrast across the boundary layer within the aquifer is less than the freshwater seawater density contrast and (2) flow into the top of the boundary is restricted relative to that in the experiment of Figure 5. The enhanced stability of the boundary layer is apparent in Figure 7 from the fact that instabilities appear a finite distance from the current coastline. Third, once the instabilities have grown into macroscopic salt fingers, they do not sink as readily as in Figure 5 because of the low-density contrast with the ambient groundwater and because of the greater resistance to drawing dense fluid from the overlying sea reservoir. Therefore a wide low-salinity transition zone develops which is intermediate in nature relative to the experiments of Figures 5 and 6. It should be noted that a minimum thickness of the sandy layer is required for instabilities to arise. Experiments 15 and 16 constrain the nondimensional critical transgression rate to occur between $\Gamma_{\text{sand}} = 0.93$ and $\Gamma_{\text{sand}} = 1.86$, which is ~5 times lower than for a pure sand substrate. A greater thickness of the clay layer will probably further reduce the critical transgression rate and result in lower salinity pore waters in the underlying aquifer. However, this was not tested within the present set of experiments. The effect of hydrodynamic dispersion was investigated in experiments 19 and 20. It was found that similar to a uniform sand substrate, hydrodynamic dispersion increases the thickness of the boundary layer and the width of the fingers but does not alter the mode of intrusion in a major way.

4. Discussion and Conclusions

4.1. Modes of Seawater Intrusion During Transgression

It is proposed that the numerical experiments of Figures 4–7 have a generic value in the sense that the behavior shown for each experiment is representative of the behavior of a whole class of experiments. This idea is based on the notion that the various behaviors exhibited by the experiments of Figures 4–7 can be readily understood from (1) the concept of a critical transgression rate discussed in section 2 and (2) theory of diffusive boundary layer stability [*Wooding et al.*, 1997]. Moreover, although we have not systematically varied all system parameters (e.g., aquifer thickness and surface gradient), the experiments which we did perform are consistent with this hypothesis. On the basis of these findings, four modes of seawater intrusion are distinguished:

1. One is quasi-steady, "horizontal" seawater intrusion in the form of landward migration of a "narrow" transition zone closely following shoreline migration (Figure 4). This mode occurs for a sufficiently slow, subcritical rate of transgression. An estimate of the critical transgression rate at which the transition to mode 2 or 3 occurs for uniform substrate conditions is given by (4). Experiments showed that (4) is accurate to one order of magnitude and tends to underestimate Γ_{cr}.
2. The next mode is vertical seawater intrusion by fingers of seawater (Figure 5). This mode occurs for supracritical transgression rates and a relatively high permeability substrate (sand/silt). A wide high-salinity transition zone develops.
3. The third mode is vertical seawater intrusion by diffusion (Figure 6). This mode occurs for supracritical transgression rates, which can be very small, and for low-permeability substrate sediments (silt/clay) up to great depth. An extensive seaward dipping freshwater wedge develops below a thick, not well mixed, mainly vertical transition zone.
4. The last mode is vertical seawater intrusion by low-salinity fingers (Figure 7). This mode occurs for supracritical transgression rates and a layer of low-permeability seafloor sediments (silt/clay) overlaying a relatively high-permeability aquifer. A wide, low-salinity, well-mixed transition zone develops in the aquifer bounded, on top, by a relatively sharp transition to seawater quality in the overlaying low-permeability layer.

Incorporation of diurnal effects, such as tides, might affect details of the predicted salinity patterns. This would apply in particular to the relatively small spatial scale of the experiments presented here. However, it seems reasonable to assume that the modes distinguished above do provide insight for much larger scales of tens to hundreds of kilometers and geological timescales for which the magnitude of sea level change overwhelms that of diurnal processes. Perhaps more important shortcomings of the modeling with respect to its applicability to natural systems are its two-dimensional character and the absence of heterogeneity in subsurface conditions. Landscapes that are transgressed by the sea are often fluvially dominated, characterized by three-dimensional relief with valleys and channels and by laterally varying substrate conditions. These factors require further investigation.

4.2. Factors Favoring Preservation of Fresh/Brackish Groundwater Offshore

The above findings provide a framework for prediction of offshore groundwater salinity patterns. Such a framework for prediction may be valuable in possible future offshore groundwater exploration, which becomes more viable as pressures on onshore groundwater resources increase. Of particular interest in this respect is the prediction of occurrences of fresh and/or brackish groundwater in subsea aquifers (Figure 1). The highest potential for such occurrences would require a combination

of (1) a low-gradient land surface/seafloor and (2) a thick clay layer overlaying a thick high-permeability aquifer. Both factors favor a low critical transgression rate (equation (4)) and mode 3 or 4 salinization. A thick clay layer both enhances the horizontal length scale over which the diffusive boundary layer is stable and reduces the salinity and diffusive input of salt in the top of the aquifer. A thick aquifer enhances the timescale of mixing by convection and diffusion. Both conditions do occur in the offshore of Suriname (Figure 1a), where the shelf gradient is ~1:1000 and extensive Tertiary aquifers are covered by a >10 m thick late Pleistocene/Holocene clay layer [*Groen et al.*, 2000]. The New Jersey continental margin (Figure 1b) has a similar shelf gradient, and *Hathaway et al.* [1979] report that at this margin the sharp chlorinity gradient separates seawater from the underlying freshwater lens in late Miocene and Pleistocene low-permeability clays. Because extensive clay layers are common beneath the middle and outer shelf of continental margins, fresh water trapped there during the Pleistocene glacial maximum and which subsequently underwent only partial salinization may be a general feature of most continental margins around the world.

Obviously, for a comprehensive appraisal of the prospects for relatively fresh groundwater in the offshore the actual history of sea level change will have to be considered. Although this is not the prime objective of the present paper, two aspects of this issue will be discussed briefly. First, in the experiments presented, sea level rise and transgression rate are assumed constant. At most continental shelf seas, away from the major ice sheets of the last ice age, transgression rates were high during the early Holocene (10,000–5000 years B.P.) and much reduced during the last 5000 years. During the latter phase the groundwater salinity distributions may have largely or partially caught up with the new shoreline location. However, these conditions do not challenge the validity of the above requirements 1 and 2 because, in general, the hydraulic conditions that favor the development of a major lag during a phase of rapid sea level rise also tend to preserve the disequilibrium salinity distribution most effectively during a subsequent phase of reduced or no transgression.

Second, the assumption of an initial steady state salinity distribution for low sea level may have an influence. This assumption would require low sea level to have been maintained for a period that is long compared to the "freshening response time" for forcing by sea level fall (the regression part of transgression-regression cycles). Although this response time needs quantification in future work, it is evident that large values of this quantity also are favored by requirements 1 and 2. Therefore prediction of salinity patterns for 1 and 2 will always be hampered by the difficulty in assigning a realistic initial condition.

Finally, it is worth noting that the values of the transgression rates of $\nu_{tr} = 0.1$ and 1.0 m/yr that were used in the experiments presented in this paper are not particularly high. Much more rapid transgression occurred in many parts of the world during the early Holocene when sea level rose rapidly relative to the land surface during the melting of the large continental ice sheets in North America and Fennoscandia. For example, the coastline of the North Sea migrated southward over a distance of ~300 km between 10,300 and 8700 years B.P. [*Jelgersma*, 1979], which yields an average value of 200 m/yr. Similar rates occurred during the formation of the former Zuiderzee embayment in the Netherlands. This inland sea was formed in medieval times by erosion of large peat areas. Once inundation started, it progressed rapidly up to some 100 km from the former coast line within a couple of centuries. A clay layer prevented massive salinization of the underlying Pleistocene aquifer during the ~700 years of existence of this inland sea before it was reclaimed and turned into a freshwater lake. Values in excess of 100 m/yr are probably typical for the early Holocene for many continental margins away from the major continental ice sheets of the last ice age.

Notation

D scalar value dispersivity (L^2/T).
D_m molecular diffusivity (L^2/T).
g scalar value gravitational acceleration (L/T^2).
$\mathbf{g}$ gravitational acceleration (L/T^2).
h sea depth (L).
k scalar value intrinsic permeability (L^2).
$\mathbf{k}$ intrinsic permeability tensor (L^2).
p fluid pressure (M/LT^2).
p_b fluid pressure top boundary node (M/LT^2).
p^* fluid pressure steady state flow regime (M/LT^2).
δp perturbation fluid pressure (M/LT^2).
$\mathbf{q}$ Darcy velocity (L/T).
$\mathbf{q}^*$ Darcy velocity steady state flow regime (L/T).
Ra_{cr} critical Rayleigh number saline boundary layer (dimensionless).
$\nu_{\text{adv}}^{\max}$ maximum pore water advection rate (L/T).
ν_{sl} rate of sea level rise (L/T).
ν_{tr} rate of transgression (L/T).
ν_{tr}^{cr} critical transgression rate (L/T).
Δx horizontal mesh size (L).
Δz vertical mesh size (L).
α_L longitudinal dispersivity (L).
α_T transversal dispersivity (L).
β gradient of topography (dimensionless).
δ_{cr} thickness critical saline boundary layer (L).
γ constant in equation of state (dimensionless).
Γ normalized transgression rate (dimensionless).
Γ^{cr} normalized critical transgression rate (dimensionless).
λ_{cr} wavelength of instability critical saline boundary layer (L).
μ dynamic viscosity (M/LT).
ρ fluid density (M/L^3).
ρ^* fluid density of steady state situation (M/L^3).
ρ_{sea} fluid density of seawater (M/L^3).
$\Delta\rho$ density difference across saline boundary layer (M/L^3).
ω salt mass fraction (dimensionless).
ω_b salt mass fraction of top boundary node (dimensionless).
ω_{sea} salt mass fraction of seawater (dimensionless).

Acknowledgments. SARA (Academic Computing Services Amsterdam) is acknowledged for permission to use their IBM SP2 for the numerical calculations. We would like to thank Craig Simmons, Mark Bakker, and an anonymous reviewer for their constructive comments which helped improve the paper. This is a contribution to the NEESDI (Netherlands Environmental Earth System Dynamics Initiative) program, funded by the Netherlands Organisation for Scientific Research (NWO-grant 750.296.01).

References

Bear, J., A. H.-D. Cheng, S. Sorek, D. Ouazar, and I. Herrera (Eds.), *Seawater Intrusion in Coastal Aquifers: Concepts, Methods and Prac-*

tices, Theory and Applications of Transport in Porous Media, vol. 14, 625 pp., Kluwer Acad., Norwell, Mass., 1999.

Custodio, E., G. A. Bruggeman, and V. Cotecchia, Groundwater problems in coastal areas, *Studies and Reports in Hydrology*, vol. 35, 650 pp., UNESCO, Paris, 1987.

De Vries, J. J., Fresh and salt groundwater in the Dutch coastal area in relation to geomorphological evolution, *Geol. Mijnbouw*, *60*, 363–368, 1981.

Elder, J. W., The unstable thermal interface, *J. Fluid Mech.*, *32*, 69–96, 1968.

Galeati, G., G. Gambolati, and S. P. Neuman, Coupled and partially coupled Eulerian-Lagrangian model of freshwater-seawater mixing, *Water Resour. Res.*, *28*, 149–165, 1992.

Groen, J., J. Velstra, and A. G. C. A. Meesters, Salinization processes in paleowaters in coastal sediments of Suriname: Evidence from δ^{37} Cl analysis and diffusion modelling, *J. Hydrol.*, *234*, 1–20, 2000.

Hathaway, J. C., C. W. Poag, P. C. Valentine, R. E. Miller, D. M. Schultz, F. T. Manheim, F. A. Kohout, M. H. Bothner, and D. A. Sangrey, U.S. Geological Survey core drilling on the Atlantic shelf, *Science*, *206*, 515–527, 1979.

Henry, H. R., Effects of dispersion on salt encroachment in coastal aquifers: Sea water in coastal aquifers, *U.S. Geol. Surv. Water Suppl. Pap.*, *1613-C*, 70–84, 1964.

Jelgersma, S., Sea-level changes in the North Sea Basin, in *The Quaternary History of the North Sea*, edited by E. Oele, R. T. E. Schuttenhelm, and A. J. Wiggers, *Symposia Univ. Upsaliensis Annum Quingentesium Celebrantis*, vol. 2, pp. 233–248, Univ. of Uppsala, Stockholm, 1979.

Kana, T. W., J. Michel, M. O. Hayes, and J. R. Jensen, The physical impact of sea level rise in the area of Charleston, South Carolina, in *Greenhouse Effect and Sea Level Rise: A Challenge for this Generation*, edited by M. C. Barth and J. G. Titus, pp. 105–150, Van Nostrand Reinhold, New York, 1984.

Kohout, F. A., J. C. Hathaway, D. W. Folger, M. H. Bothner, E. H. Walker, D. F. Delaney, M. H. Frimpter, E. G. A. Weed, and E. C. Rhodehamel, Fresh ground water stored in aquifers under the continental shelf: Implications from a deep test, Nantucket Island, Massachusetts, *Water Resour. Bull.*, *13*, 373–386, 1977.

Kolditz, O., R. Ratke, H.-J. G. Diersch, and W. Zielke, Coupled groundwater flow and transport, 1, Verification of variable density flow and transport models, *Adv. Wat. Resour.*, *21*, 27–46, 1998.

Leijnse, A., Three-dimensional modeling of coupled flow and transport in porous media, Ph.D. thesis, 251 pp., Notre Dame Univ., Indiana, 1992.

Leijnse, A., and S. M. Hassanizadeh, Verification of the METROPOL code for density dependent flow in porous media, Hydrocoin project level 2 case 2, *RIVM Rep. 728528002*, Natl. Inst. of Public Health and Environ Prot., Bilthoven, Netherlands, 1989a.

Leijnse, A., and S. M. Hassanisadeh, Verification of the METROPOL code for density dependent flow in porous media, Hydrocoin project level 1 case 5 and level 3 case 4, *RIVM Rep. 728528004*, Natl. Inst. of Public Health and Environ. Prot., Bilthoven, Netherlands, 1989b.

Leijnse, A., and M. Oostrom, The onset of instabilities in the numerical simulation of density-driven flow in porous media, in *Computational Methods in Water Resources X*, edited by A. Peters et al., pp. 1011–1018, *Kluwer Acad.*, Norwell, Mass., 1994.

Manheim, F. T., and M. K. Horn, Composition of deeper subsurface waters along the Atlantic continental margin, *Southeast Geol.*, *9*, 215–236, 1968.

Manheim, F. T., and C. K. Paull, Patterns of groundwater salinity changes in a deep continental-oceanic transect off the southeastern Atlantic coast of the U.S.A., *J. Hydrol.*, *54*, 95–105, 1981.

Meisler, H., P. P. Leahy, and L. L. Knobel, Effect of eustatic sea-level changes on saltwater-freshwater in the northern Atlantic coastal plain, *U.S. Geol. Surv. Water Supply Pap.*, *2255*, 1984.

Navoy, A. S., Aquifer-estuary interaction and vulnerability of groundwater supplies to sea level rise-driven saltwater intrusion, Ph.D. thesis, 225 pp., Pa. State Univ., University Park, 1991.

Oostrom, M., A. Leijnse, and K. R. Roberson, Simulation of two- and three-dimensional dense solute plume behavior with the METROPOL-3 code, in *Computational Methods in Water Resources X*, edited by A. Peters et al., pp. 975–982, Kluwer Acad., Norwell, Mass., 1994.

Oude Essink, G. H. P., Impact of sea level rise on groundwater flow regimes: A sensitivity analysis for the Netherlands, Ph.D. thesis, 411 pp., Delft Univ. of Technol., Delft, Netherlands, 1996.

Oude Essink, G. H. P., Impact of sea level rise in the Netherlands, in *Seawater Intrusion in Coastal Aquifers: Concepts, Methods and Practices, Theory and Applications of Transport in Porous Media*, vol. 11, edited by J. Bear et al., pp. 507–530, Kluwer Acad., Norwell, Mass., 1999.

Reilly, T. E., and A. S. Goodman, Quantitative analysis of saltwater-freshwater relationships in groundwater systems—A historical perspective, *J. Hydrol.*, *80*, 125–160, 1985.

Sauter, F. J., A. Leijnse, and A. H. W. Beusen, Metropol's user's guide, *RIVM Rep. 725205003*, Natl. Inst. of Public Health and Environ. Prot., Bilthoven, Netherlands, 1993.

Simmons, C. T., K. A. Narayan, and R. A. Wooding, On a test case for density-dependent groundwater flow and solute transport models: The salt lake problem, *Water Resour. Res.*, *35*, 3607–3620, 1999.

Souza, W. R., and C. I. Voss, Analysis of an anisotropic coastal aquifer system using variable-density flow and solute transport simulation, *J. Hydrol.*, *92*, 17–41, 1987.

Volker, R. E., and K. R. Rushton, An assessment of the importance of some parameters for seawater intrusion in aquifers and a comparison of dispersive and sharp-interface modelling approaches, *J. Hydrol.*, *56*, 239–250, 1982.

Voss, C. I., and W. R. Souza, Variable density flow and solute transport simulation of regional aquifers containing a narrow freshwater-saltwater transition zone, *Water Resour. Res.*, *23*, 1851–1866, 1987.

Wooding, R. A., S. W. Tyler, and I. White, Convection in groundwater below an evaporating salt lake, 1, Onset of instability, *Water Resour. Res.*, *33*, 1199–1217, 1997.

J. Groen and H. Kooi, Faculty of Earth Sciences, Vrije Universiteit, De Boelelaan 1085, 1081 HV Amsterdam, Netherlands. (kooi@geo.vu.nl)

A. Leijnse, National Institute of Applied Geosciences, P.O. Box 80015, 3508TA, Utrecht, Netherlands.

(Received February 16, 2000; revised August 7, 2000; accepted August 8, 2000.)